Reconfigurable chessboard coding plasma-based dielectric resonator structure for RCS reduction

Hend Abd El-Azem Malhat[1] · Anas Saber Zainud-Deen[2] · Mona Magdy Badawy[1]

Abstract

In this paper, reconfigurable chessboard coding plasma-based dielectric structure for radar cross section reduction is investigated. The radar cross section (RCS) reduction is essential in military applications. The metallic conductor surface is covered with plasma-based dielectric resonator (DRA) unit-cells arranged in chessboard configuration. The plasma DRA unit-cell consists of concentric cylindrical ring filled with ionized plasma placed over FR4 dielectric substrate. The plasma ionization voltage values are tuned to reflect the electromagnetic wave with phase shift of 180° and equal amplitudes. The phase 0° state represents the logic "0" while the phase 180° state represents the logic "1". The chessboard arrangement consists of super-cells with 0/1 logic states. Different sizes of uniform super-cells 3×3, 4×4, 6×6, and 12×12 unit-cells are investigated for maximum RCS reduction. The scattered beams are directed to ($\pm 30°$, $180° \pm 30°$), ($\pm 25°$, $180° \pm 25°$), ($\pm 20°$, $180° \pm 20°$), ($\pm 15°$, $180° \pm 15°$) and ($\pm 10°$, $180° \pm 10°$) for 3×3, 4×4, 6×6, 8×8, and 12×12 uniform super-cells, respectively. The RCS is reduced over a wide angle range reduction with -18 dBm^2 at the broadside direction and below -32 dBm^2 over the angular range from $-90°$ to 90° according to the super-cell size. The non-uniform allocation of unit-cells in the super-cell chessboard arrangement is investigated. The RCS reduction bandwidth extended from 8.5 to 9.65 GHz. The scattered beam produces null in the broadside direction with wideband RCS reduction. The proposed structures are simulated using CST-MWS electromagnetic simulator.

Keywords RCS reduction · Coding · Chessboard arrangement · Scattering

✉ Hend Abd El-Azem Malhat
   er_honida1@yahoo.com

   Anas Saber Zainud-Deen
   anas-saber@eru.edu.eg

   Mona Magdy Badawy
   eng_mona201060@yahoo.com

[1] Department of Electronics and Electrical Communication Engineering, Faculty of Electronic Engineering, Menoufia University, Menouf, Egypt

[2] Telecommunication Engineering Department, Faculty of Engineering, Egyptian Russian University, ERU, Cairo, Egypt

1 Introduction

The main consideration in the design of military platforms is the reduction of radar coverage (RCS). Two methods for RCS reduction are commonly available in the literature: changing the object structure to redirect the scattered waves away from the incidence direction and loading radar absorbing material (RAM) on the object (Singh and Jha 2015; Cos et al. 2010). The drawbacks of both methods are a complex design, large volume and small bandwidth. Meta-surfaces have been adopted to overcome the aforementioned drawbacks. The RCS reduction can be achieved while using meta-surfaces consisting of equivalent perfect electric conductors (PEC) and artificial magnetic conductors (AMC) unit cells. Metamaterial provides a new way to manipulate electromagnetic (EM) waves and achieves the broadband and low-reflection materials. In many situations, the application scope of the three-dimensional (3D) metamaterials is limited due to their large volumes. The meta-surface is a 2D equivalent of metamaterials (Singh and Marwaha Jan 2015), which are usually constituted by inhomogeneous arrays of sub wavelength resonators. However, once the structure-only metamaterials (i.e. passive metamaterial) are fabricated, their functions will be fixed. To control the EM waves dynamically, active devices are integrated into the structure, yielding active metamaterials. Traditionally, the active metamaterials include tunable metamaterials and reconfigurable metamaterials, which have either small-range tenability or a few numbers of reconfigurability. Recently, a special kind of active metamaterials, digital coding and programmable metamaterials, haven been presented, which can realize a large number of distinct functionalities and switch them in real time with the aid of field programmable gate array (FPGA). Coding metamaterials offered a novel way to manipulate the backscatter performance by different codes (Hao et al. 2019). Several methods have been used to reduce the backscatter using metamaterial (Cos et al. 2010; Failed 2018; Zhang et al. 2012). In these methods, the meta-surface enables high efficiency propagating-wave to surface-wave conversion, deflected reflection, or diffused reflection if appropriately designed. The chessboard surface is another essential technique for RCS reduction. The chessboard surface is similar to shaping technology, and the design of chessboard configuration is easier. The working mechanism of the chessboard artificial magnetic conductor (AMC) for RCS reduction is that the backscattered field will cancel when the phase difference of the reflected fields between the two kinds of AMC units is 180°. Paguay et. al combined perfect electric conductor (PEC) and AMC in chessboard arrangement in Paquay et al. (2007). The reflect energy was scattered into four diagonal directions, and the RCS in the normal direction was almost zero. A method utilized two kinds AMC units is proposed in Chen et al. (2015). Tao et al. put two kinds of AMC units cell in triangle arrangement in Song et al. (2018). Chen et.al put the same units in different sizes randomly in Chen et al. (2017), which redistributed the scattering energy from the surface toward all the directions. Coding metamaterials concept is proposed by Cui et.al, realize different functionalities by means of biased diode, field-programmable gate array (FPGA) and different codes in Giovampaola and Engheta (2014).

In this paper, different configured chessboard plasma-based DRA is proposed by increasing the number of interfaces between adjacent unit-cells and thus redirecting the incident wave into different reflected lobes. As a result, the RCS is highly attenuated. The size of super-cell is investigated for RCS reduction over the operating bandwidth. Different arrangements of super-cells with uniform and non-uniform coding arrangements are investigated.

2 Design of plasma-based DR unit-cell

The detailed configuration of the proposed plasma-based dielectric resonator (DR) unit-cell structure is shown in Fig. 1a. It consists of dielectric container of dielectric constant $\varepsilon_{rc} = 3.4$ with cylindrical core of radius $R_o = 3$ mm, surrounded by cylindrical ring of radius $R_1 = 5$ mm, width $W_1 = 0.82$ mm, and height $H_c = 1.2$ mm. The dielectric container is placed on $L_s \times L_s \times H_s = 15 \times 15 \times 2$ mm³ grounded FR4 substrate of $\varepsilon_{rd} = 4.6$ and $tan\delta = 0.036$. The container is injected with argon-noble gas occupying a height of $H_p = 1$ mm and connected with voltage source for plasma ionization. The dispersive plasma material characteristics is calculated from Malhat et al. Oct. (2015):
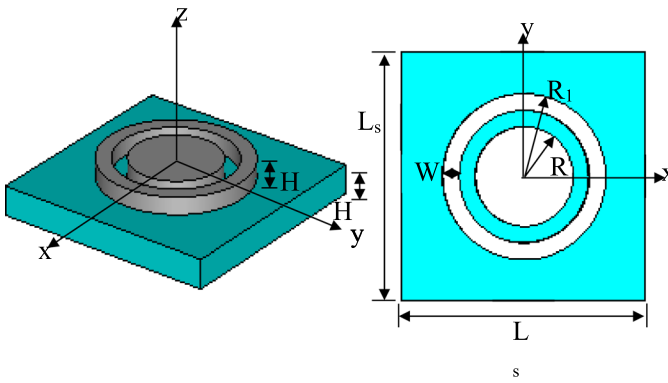
a. Unit-cell construction
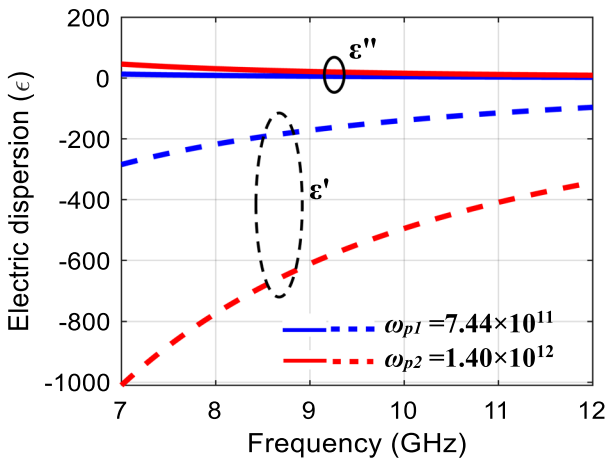
b. Plasma dispersion properties

Fig.1 a The configuration of the reconfigurable plasma ring unit-cell. **b** The dispersion properties of the plasma material

$$\varepsilon = \varepsilon_o \left[1 - \frac{\omega_p^2}{\omega(\omega - jv_p)} \right] \tag{1}$$

where ε_o is the free space permittivity, ω is the angular operating frequency, v_p is the collision frequency, and ω_p is the plasma angular frequency which is related to the electron density n_e as

$$\omega_p = \sqrt{\frac{n_e e^2}{m_e \varepsilon_o}} \tag{2}$$

where e and m_e are the electron charge and mass. The electron density of the ionized plasma medium is controlled by the applied voltage as given by Zainud-Deen et al. Dec. (2019)

$$V_B = \left(\frac{n_e \sqrt{ekT_e} H_p^2}{\varepsilon_0} \right)^{2/3} \tag{3}$$

where K is Boltzmann constant, and T_e is the electron temperature. Figure 1b shows the frequency response of plasma dispersive properties for v_p=2 GHz and T_e=300 K at ω_{p1} =7.44×10^{11} rad/sec and ω_{p2}=1.4×10^{12} rad/sec. In the frequency range from 7 to 12 GHz, the real part of dielectric constant is increased while the imaginary part is decreased with increasing the operating frequency. The plasma conductivity is decreased with increasing the operating frequency, while it has a tunable response with varying the plasma frequency. At fixed frequency of 9.5 GHz, the plasma conductivity is increased with increasing ω_p from 7.44×10^{11} to 1.4×10^{12} rad/sec. The frequency response of the reflection coefficient is calculated using the waveguide simulator at ω_{p1}=7.44×10^{11} rad/sec and ω_{p2} =1.4×10^{12} rad/sec as shown in Fig. 2a. The zero-crossing frequency of the reflection phase curve are 9.2 GHz and 10 GHz, for ω_{p1} and ω_{p2} respectively. The reflection phase difference is 180° ± 37° within the range between 9.2 and 9.8 GHz. At 9.5 GHz the two unit cells have identical reflective amplitudes of −4 dB and opposite reflective phases of 180°. The structure with ω_{p1} denotes logic "0" and the other with ω_{p2} denotes logic "1". Figure 2b shows the arrangement of uniform super-cell consists of 4×4 plasma DR unit-cell used as a building block of RCS reduction surfaces.

3 RCS reduction theory of operation

To reduce the scattered field from metallic plate surface, it is covered by the plasma DR unit-cell elements energized into two different plasma frequencies, ω_{p1} and ω_{p2} called coding configuration. When illuminated by normal incident plane- wave, the scattered fields are directed into different directions according to the reflection phases of the plasma DR elements (i.e. coding configurations). The scattering field pattern from 2-D coding-surface is calculated using the antenna array principles given by,
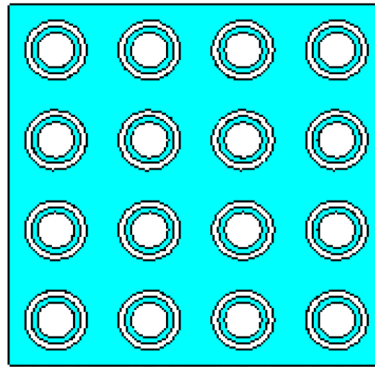
$$F(\theta, \phi) = \text{field of reference element} \times \text{array factor} \tag{4}$$

The array factor M×N array elements is expressed by

Fig. 2 a The reflection coefficient phase and magnitude for logic 0 and 1 versus frequency, **b** The geometry for 4×4 uniform super-cell
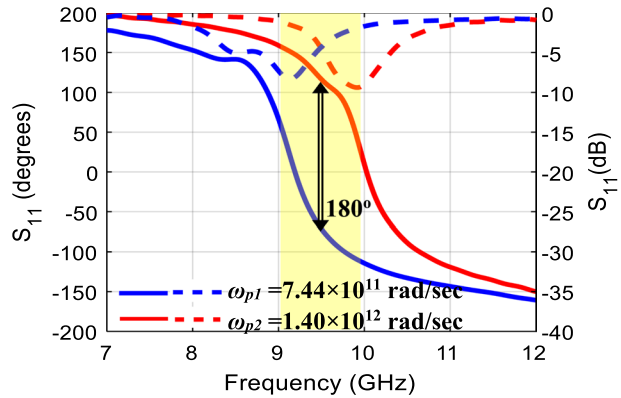
a.   Reflection phase/magnitude

b. 4×4 uniform super-cell

$$AF(\theta, \phi) = \sum_{m=1}^{M} \sum_{n=1}^{N} \exp j\left[\phi_{m,n} + \beta D_x\left(m - \frac{1}{2}\right)(u - u_o) + \beta D_y\left(n - \frac{1}{2}\right)(v - v_o)\right] \quad (5)$$

where $u = sin\theta\ cos\phi, v = sin\theta\ sin\phi, u_o = sin\theta_i\ cos\phi_i, v_o = sin\theta_i\ sin\phi_i$, θ_i is the pitching angle of incident wave and ϕ_i is the azimuth angle of incident wave. Supposing that $\phi_{m,n}$ of coding unit-cell element "1" has the value of π, $\phi_{m,n}$ of coding unit-cell element "0" has the value of 0, Eq. (5) is then rewritten as

$$AF(\theta, \phi) = \sum_{m=1}^{M} \exp j[\beta D_x\left(m - \frac{1}{2}\right)(u - u_o) + m\pi] + \sum_{n=1}^{N} \exp j\left[\beta D_y\left(n - \frac{1}{2}\right)(v - v_o) + n\pi\right]$$
$$(6)$$

The amplitude of the $AF(\theta, \phi)$ is deduced as

$$|AF(\theta, \phi)| = MN sinc\left(\frac{m\pi}{2} - \frac{m}{2}\beta D_x(u - u_o) + pm\pi\right) + sinc\left(\frac{n\pi}{2} - \frac{n}{2}\beta D_y(v - v_o) + qn\pi\right)$$
$$(7)$$

in which $sinc(x) = \frac{sin(x)}{x}$, D_x and D_y are the inter-element distance in x- and y-direction and p, $q = 0, \pm 1, \pm 2, \ldots..$ It is clear that, under normal incidence, the maximum values of $|AF(\theta, \phi)|$ appears at the direction of elevation angles

$$\phi = \pm atan\frac{D_x}{D_y} and \; \phi == \pi \pm atan\frac{D_x}{D_y} \tag{8}$$

And azimuth angle

$$\theta = asin[\frac{\lambda}{2}\sqrt{\frac{1}{D_x^2} + \frac{1}{D_y^2}}] \tag{9}$$

These expressions indicate the possibility to realize the beam sweeping at the same frequency by changing the super-cell size and the distribution of the digital codes.

Figure 3a shows the arrangement of 6×6 uniform super-cells (24×24 unit-cells) with all unit-cells are energized using $\omega_{p2} = 1.40 \times 10^{12}$ rad/sec to represent the uniform coding sequence "1". The normal incidence plane-wave is mainly reflected to a single main beam at broadside with a scattering level of …dBm², as depicted from the 3D RCS pattern at 9.5 GHz shown in Fig. 3b. Figure 3c shows the backscattering versus frequency for the unloaded metallic plate and the loaded plate with coding structure "1". Using the coding structure "1", the RCS reduction varies from -1 dBm² to -7 dBm2 at different frequencies from the unloaded case. Figure 4a shows the periodic sequence of 111,111/000000, the normal incident plane wave is mainly reflected to two symmetrical beams. The black patches denote logic "0" and the white patches denote logic "1". The 3-D RCS at 9.5 GHz shown in Fig. 4b indicates that the two beams are directed to $-15°$ and at $+15°$,

Fig. 3 The bistatic RCS from code (111111….) 6×6 super-cells using all (1) 4×4 uniform super-cell. **b** The 3-D RCS versus angle at 9.5 GHz, **c** The back-scattering versus frequency
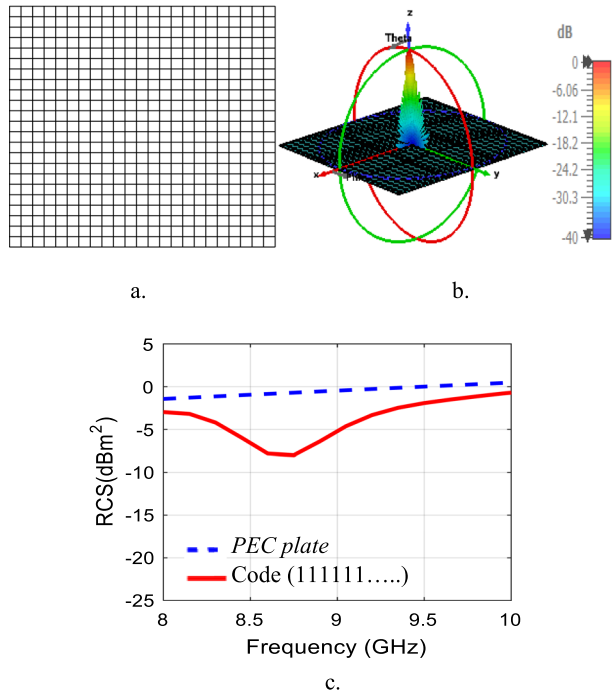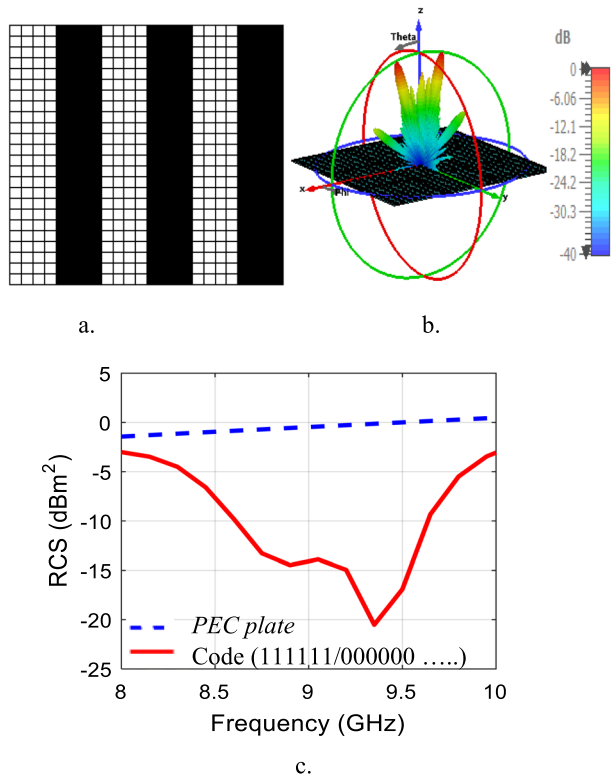
Fig. 4 The bistatic RCS from code (111111/000000….) 6×6 plasma ring surface using 4×4 uniform super-cell. **b** The 3-D RCS versus angle at 9.5 GHz, **c** The backscattering versus frequency


a.

b.

c.

respectively. The backscattering versus frequency in Fig. 4c shows a high RCS reduction over the frequency band with -21 dBm^2 at 9.4 GHz and -10 dBm^2 reduction bandwidth from 8.6 to 9.7 GHz using the 111,111/000000 coding structures. Figure 5a shows a periodic sequence of 010101/101010 chessboard arrangement. The normal incident plane wave is mainly reflected to four symmetrical beams as shown in Fig. 5b. The main lobes are directed to 45°, 135°, 225°, and 315°. The backscattering has a minimum reduction RCS of -18 dBm^2 with -10 dBm^2 reduction bandwidth extends from 8.65 to 9.75 GHz as shown in Fig. 5c.

A. RCS reduction using uniform coding supper-cells

The effect of changing the size of the super-cell consisting of uniform identical plasma DR unit-cells on the direction of the main scattered beams is explained in this section. The size of the super-cell is adjusted to control the beam directions of periodic coding patterns and the level of random diffusions. The super-cells are consisting of 3×3, 4×4, 6×6, 8×8, and 12×12 plasma DR unit-cells. The RCS from uniform super-cells ionized using $\omega_{p1}=7.44\times10^{11}$ rad/sec and $\omega_{p2}=1.4\times10^{12}$ rad/sec at 9.5 GHz are plotted in Fig. 6a and b, respectively. In both cases, increasing the super-cell size increases the RCS reflected in the illumination direction and the beam width is decreased. The peak RCS is -15.1 dBm^2, -3.97 dBm^2, and 6.43 dBm^2 for 3×3, 6×6, and 12×12 super-cells arrangements at ω_{p1}

Fig. 5 The bistatic RCS from code (010101/101010) 6×6 plasma ring surface using 4×4 uniform super-cell. **b** The 3-D RCS versus angle at 9.5 GHz, **c** The backscattering versus frequency

a.

b.

c.
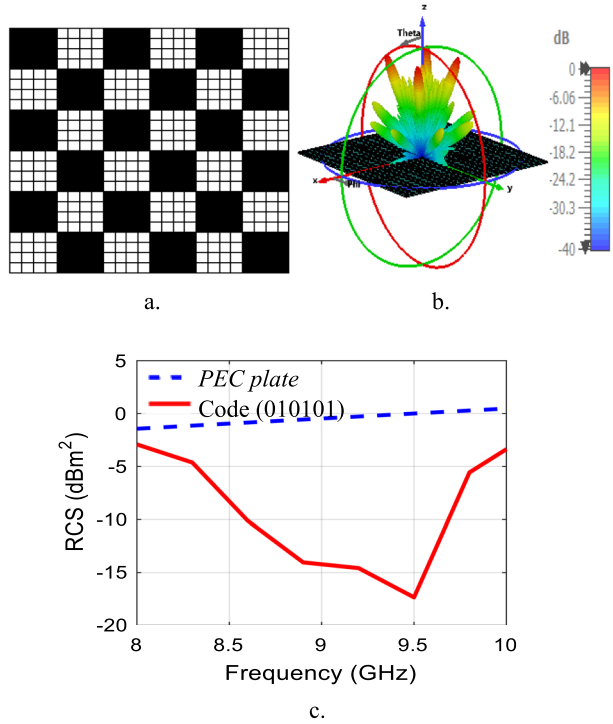
$=7.44 \times 10^{11}$ rad/sec and the RCS is -19 dBm^2, -5.93 dBm^2, and 2.88 dBm^2 for 3×3, 6×6, and 12×12 super-cells at $\omega_{p2}=1.4 \times 10^{12}$ rad/sec. Figure 7 introduces the scattering properties of chessboard arrangement of coding sequence of 101010/010101 using different sizes of uniform super-cell. For different sizes of the super-cells, the scattered field is splinted into four beams with deflection angle decrease with increasing the super-cell size. The scattered beams are directed to $(\pm 30°, 180° \pm 30°)$, $(\pm 25°, 180° \pm 25°)$, $(\pm 20°, 180° \pm 20°)$, $(\pm 15°, 180° \pm 15°)$ and $(\pm 10°, 180° \pm 10°)$ for 3×3, 4×4, 6×6, 8×8, and 12×12 uniform super-cells, respectively. The RCS is reduced over a wide angle range reduction with -18 dBm^2 at the broadside direction and below -32 dBm^2 over the angular range from $-90°$ to $90°$ according to the super-cell size. The frequency responses of the backscattered RCS are plotted in Fig. 8a. Changing the super-cell size doesn't affect the RCS reduction values where all the super-cell sizes share the same RCS reduction bandwidth from 8.7 to 9.8 GHz with highest reduction of -23 dBm^2 at 9.4 GHz. Figure 8b shows the bistatic RCS versus angle in the plane $\varphi = 45°$ for different uniform super-cell sizes. The deflected beam angle is increased with reducing the super-cell size. The deflected RCS beam amplitude is decreased by -2 dBm^2 with decreasing the super-cell size.

2   RCS reduction using non-uniform coding supper-cells

In this case, non-uniform super-cells consists of 8×8 plasma DR unit-cells ionized non-uniformly using $\omega_{p1}=7.44 \times 10^{11}$ rad/sec and $\omega_{p2}=1.4 \times 10^{12}$ rad/sec in different

3×3 uniform super-cell

3×3 uniform super-cell

6×6 uniform super-cell

6×6 uniform super-cell

12×12 uniform super-cell

12×12 uniform super-cell

a. Logic (0) with $\omega_{p1} = 7.44 \times 10^{11}$

b. Logic (1) with $\omega_{p2} = 1.40 \times 10^{12}$
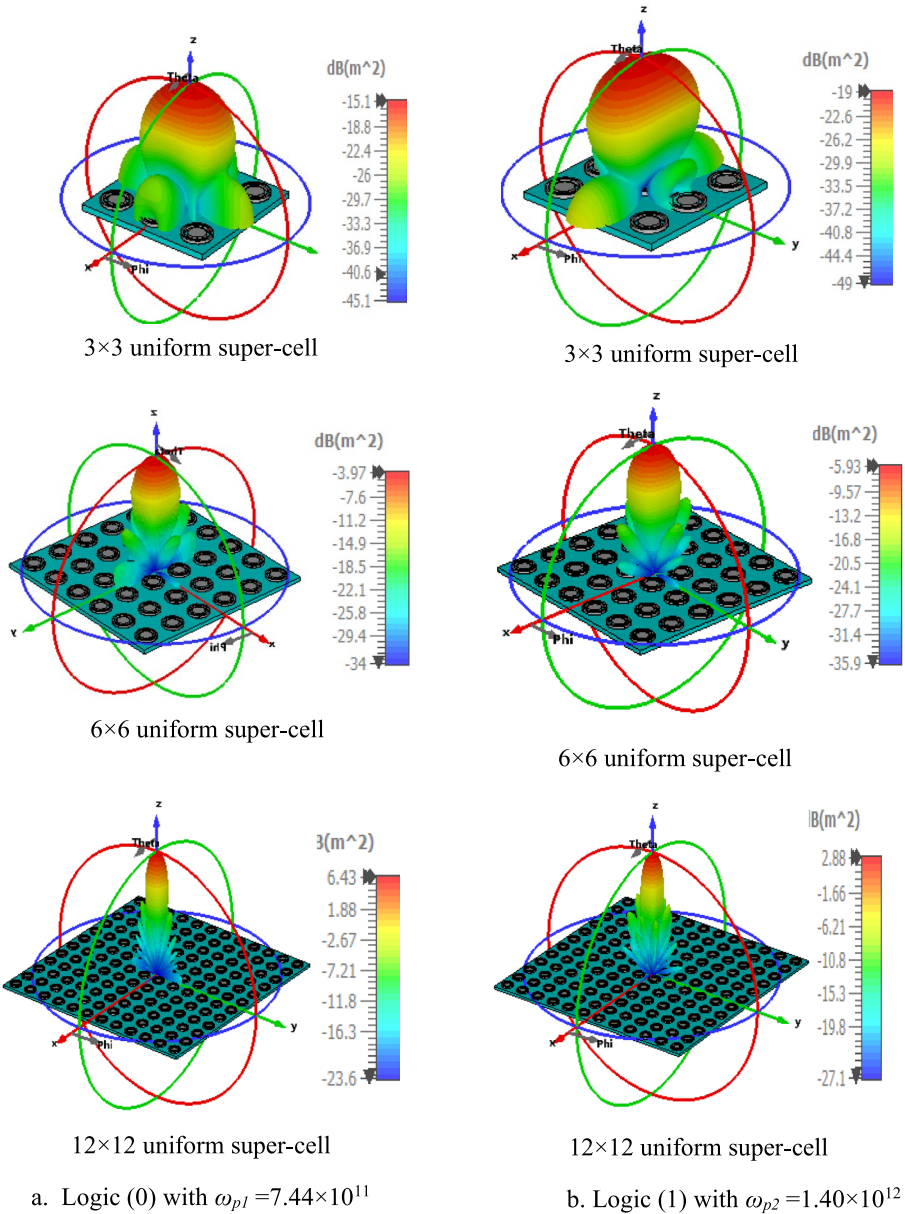
Fig. 6 The 3D-RCS from uniform super-cells with different sizes at 9.5 GHz

arrangement are considered. Figure 9 shows the RCS from different non-uniform super-cell using 8×8 plasma DR unit-cells configurations size at 9.5 GHz. The RCS varies between 2.9 and 3.19 dBm^2 for different configurations. Figure 10 introduces the RCS characteristics from 3×3 super-cells with individual 24×24 plasma DR unit-cells. The super-cells are arranged in checkboard like format to satisfy 180° progressive phase

Code arrangement   3D-RCS at 9.5 GHz

Bistatic scattering versus angle at 9.5 GHz

a.   Reconfigurable coding structure using 3×3 uniform super-cell arrangement.

Code arrangement   3D-RCS at 9.5 GHz

Bistatic scattering versus angle at 9.5 GHz

b. Reconfigurable coding structure using 4×4 uniform super-cell arrangement.

Code arrangement   3D-RCS at 9.5 GHz

Bistatic scattering versus angle at 9.5 GHz

c. Reconfigurable coding structure using 6×6 uniform super-cell arrangement.

Code arrangement   3D-RCS at 9.5 GHz

Bistatic scattering versus angle at 9.5 GHz

d. Reconfigurable coding structure using 8×8 uniform super-cell arrangement.

Code arrangement   3D-RCS at 9.5 GHz

Bistatic scattering versus angle at 9.5 GHz

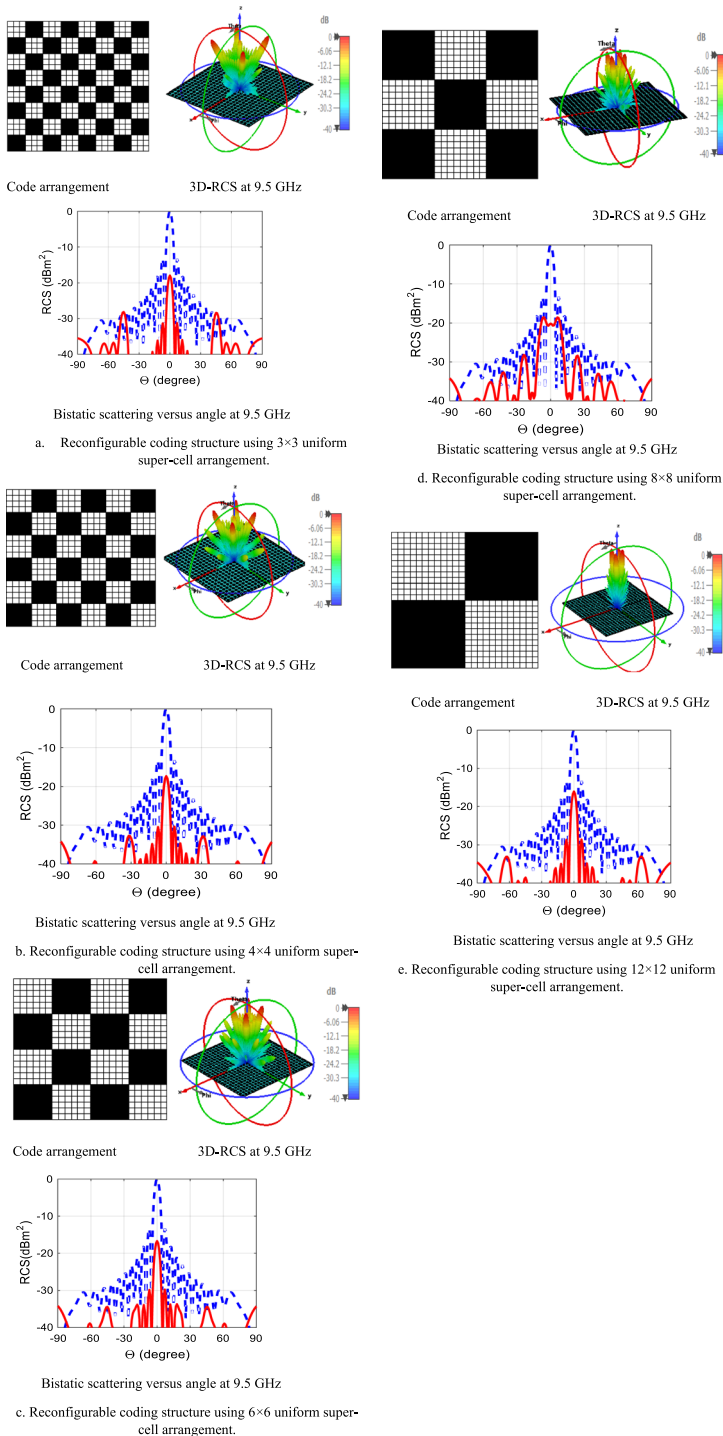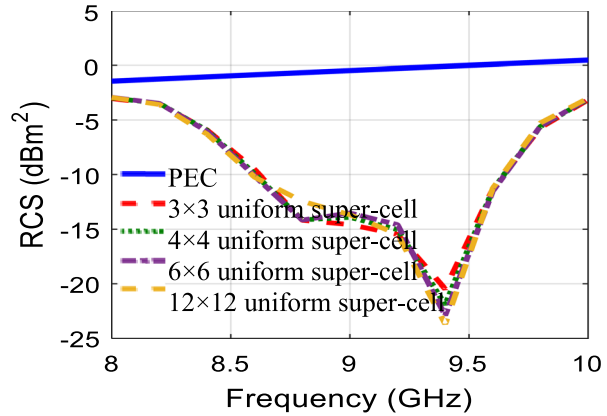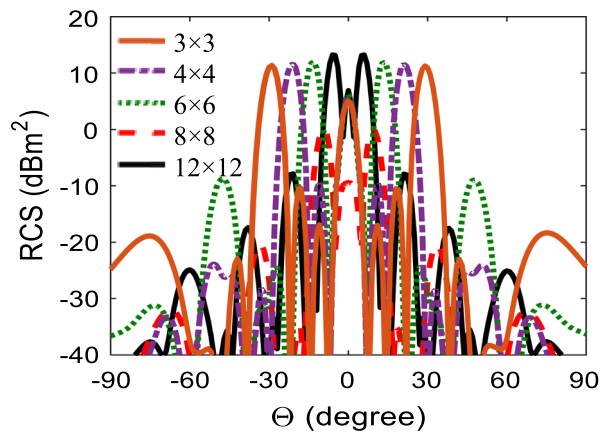e. Reconfigurable coding structure using 12×12 uniform super-cell arrangement.

Fig. 7 The RCS response from 6×6 reconfigurable coding structure consisting of different sizes of uniform super-cells

Fig. 8 **a** The backscattered RCS versus frequency. **b** The scattered beam angle versus size of super-cell at 9.5 GHz

a.

b.

criteria to result in null in boresight direction under the normal incidence waves. In Fig. 10a, super-cell arrangement (1) consists of triangle-type checkerboard surface, two opposite triangle are excited using $\omega_{p1}=7.44\times10^{11}$ rad/sec and the opposite triangles are excited using $\omega_{p2}=1.4\times10^{12}$ rad/sec. The backscattered RCS shows wideband reduction of 1 GHz with peak reduction of -17 dBm^2. The 3-D RCS shows null at the broadside direction. In super-cell arrangement (2), H-shaped unit-cells are excited using ω_{p1} and the surrounding unit-cells are excited using ω_{p2} as in Fig. 10b. Wideband RCS reduction of -15 dBm^2 over the reduction bandwidth of 1.2 GHz with scattered beams in different directions. Figure 10c shows the arrangement of super-cell (3) in which the unit-cells are diagonally divided into two triangles excited using two frequencies, ω_{p1} and ω_{p2}. The RCS reduction bandwidth extended from 8.5 to 9.65 GHz. The scattered 3D RCS pattern at 9.5 GHz shows two beams at $\pm20°$. The arrangements using super-cell (4), super-cell (5) and super-cell (6) in which different distributions of excited unit-cells are depicted in Fig. 10d, e and f, respectively. The scattered beam produces null in the broadside direction with wideband RCS reduction.
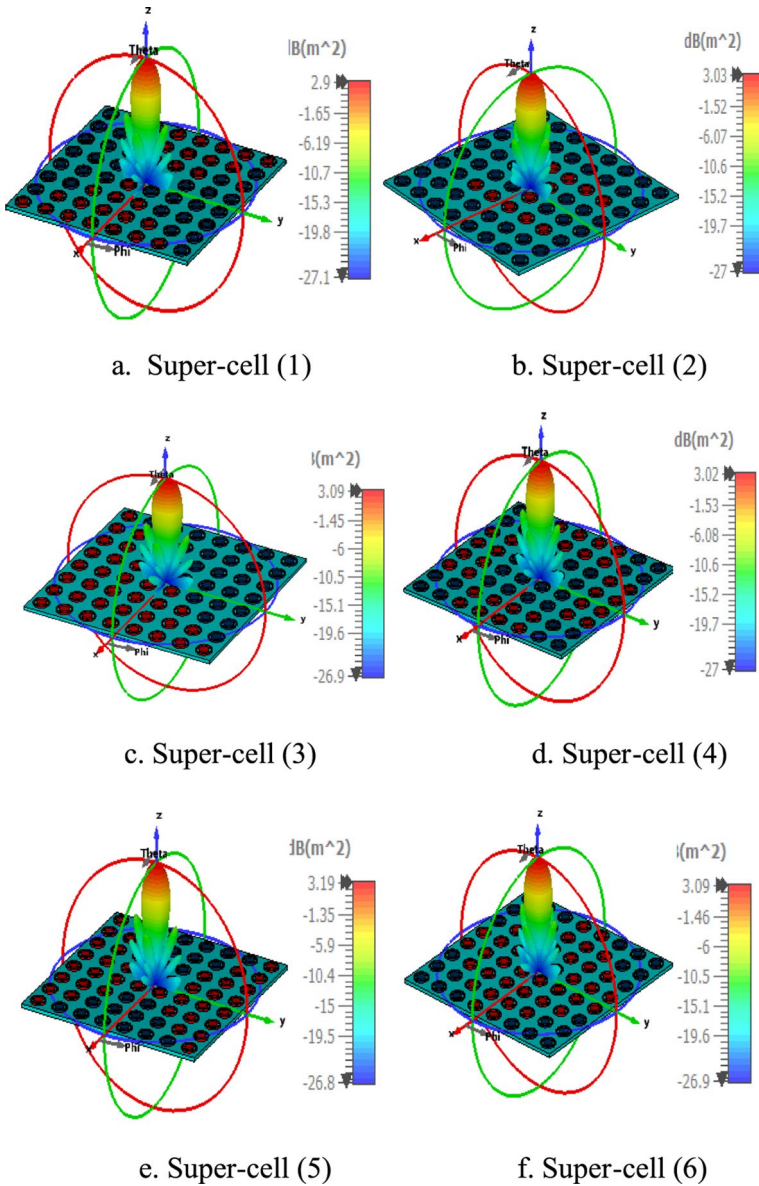
a. Super-cell (1)   b. Super-cell (2)

c. Super-cell (3)   d. Super-cell (4)

e. Super-cell (5)   f. Super-cell (6)

Fig. 9 The 3D-RCS from non-uniform super-cells at 9.5 GHz

4 Conclusion

The RCS reduction using plasma DR unit-cells chessboard arrangement is investigated in this paper. The scattering from the unit-cell is tuned using the plasma frequency with 180° degrees phase shift. The logic "0" state and logic "1" state are achieved using $\omega_p = 7.44 \times 10^{11}\,rad/sec$ and $\omega_p = 1.4 \times 10^{12}\,rad/sec$, respectively. The reflection phase
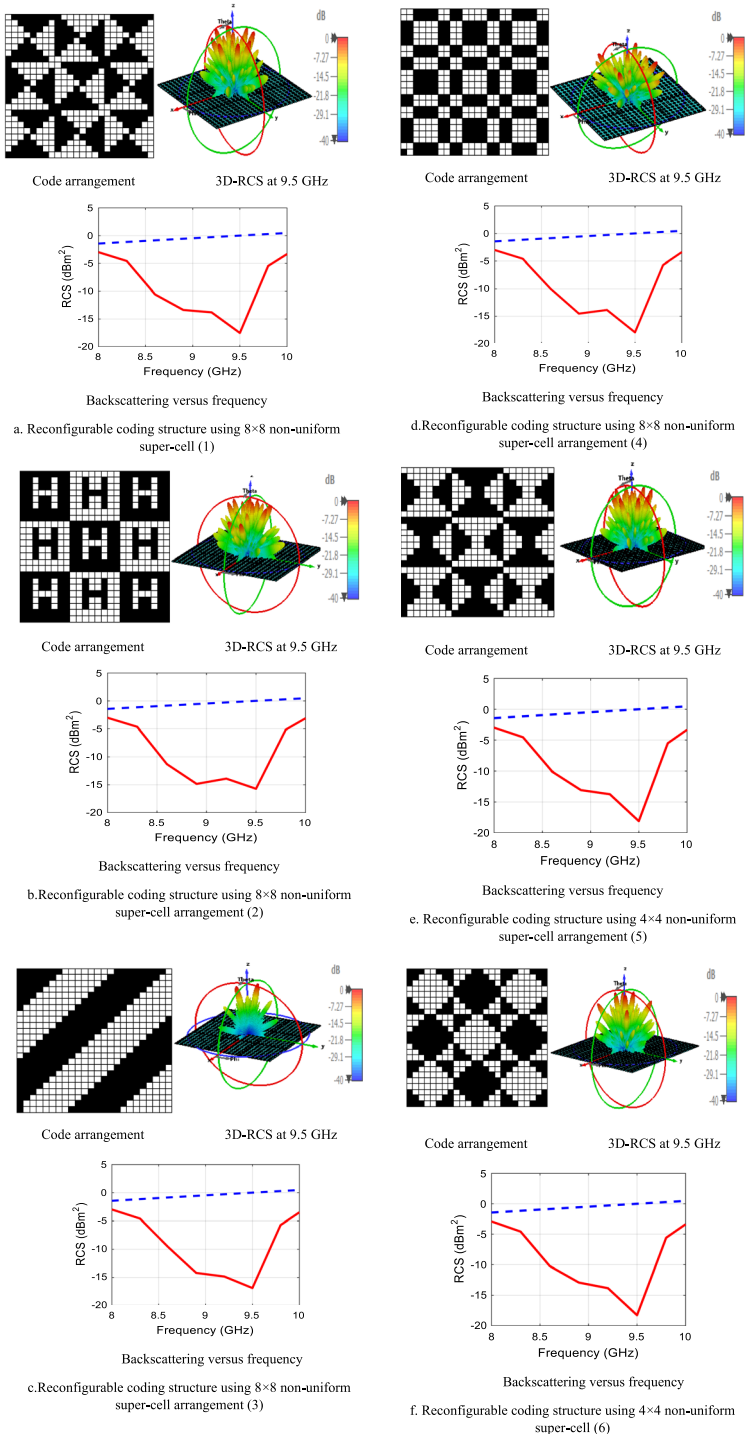
Code arrangement   3D-RCS at 9.5 GHz

Backscattering versus frequency

a. Reconfigurable coding structure using 8×8 non-uniform super-cell (1)

Code arrangement   3D-RCS at 9.5 GHz

Backscattering versus frequency

d. Reconfigurable coding structure using 8×8 non-uniform super-cell arrangement (4)

Code arrangement   3D-RCS at 9.5 GHz

Backscattering versus frequency

b. Reconfigurable coding structure using 8×8 non-uniform super-cell arrangement (2)

Code arrangement   3D-RCS at 9.5 GHz

Backscattering versus frequency

e. Reconfigurable coding structure using 4×4 non-uniform super-cell arrangement (5)

Code arrangement   3D-RCS at 9.5 GHz

Backscattering versus frequency

c. Reconfigurable coding structure using 8×8 non-uniform super-cell arrangement (3)

Code arrangement   3D-RCS at 9.5 GHz

Backscattering versus frequency

f. Reconfigurable coding structure using 4×4 non-uniform super-cell (6)

Fig. 10 The RCS response from 6×6 reconfigurable coding structure consisting of 4×4 non-uniform super-cells arrangements

difference is $180° \pm 37°$ within the range between 9.2 and 9.8 GHz. At 9.5 GHz the two unit-cells have identical reflective amplitudes of -4 dB and opposite reflective phases of $180°$. Different chessboard arrangements of uniform plasma DR unit-cells are investigated. High RCS reduction over the frequency band with -21 dBm^2 at 9.4 GHz and -10 dBm^2 reduction bandwidth from 8.6 to 9.7 GHz using the 111111/000000 coding structures. Super-cells consisting of 3×3, 4×4, 6×6, 8×8, and 12×12 plasma DR unit-cells are investigated. Increasing the super-cell size increases the RCS reflected in the illumination direction and the beam width is decreased. The RCS is reduced over a wide angle range reduction with -18 dBm^2 at the broadside direction and below -32 dBm^2 over the angular range from $-90°$ to $90°$ according to the super-cell size. Non-uniform super-cells consisting of 8×8 plasma DR unit-cells are investigated. The RCS reduction bandwidth extended from 8.5 to 9.65 GHz. The scattered 3D RCS pattern at 9.5 GHz shows two beams at $\pm 20°$ and produces null in the broadside direction with wideband RCS reduction.

Declarations

Conflict of interest The authors have no conflicts of interest or competing interests to declare that are relevant to the content of this article.

Ethical approval There is no ethical approval is required. 'Not applicable'.

Consent to participate Informed consent was obtained from all individual participants included in the study. 'Not applicable'.

Consent for publication Authors are responsible for correctness of the statements provided in the manuscript.

References

Chen, W., Balanis, C.A., Birtcher, C.R.: Checkerboard EBG surfaces for wideband radar cross section reduction. IEEE Trans. Antennas Propag. **63**(6), 2636–2645 (2015)

Chen, K., Cui, L., Feng, Y., Zhao, J., Jiang, T., Zhu, B.: Coding metasurface for broadband microwave scattering reduction with optical transparency. Opt. Express **25**(5), 5571–5579 (2017)

de Cos, M.E., Alvarez, Y., Las-Heras, F.: A novel approach for RCS reduction using a combination of artificial magnetic conductors. Prog. Electromagn. Res. **107**, 147–159 (2010)

Giovampaola, C.D., Engheta, N.: Digital metamaterials. Nat. Mater. **13**(12), 1115–1121 (2014)

Hao, H., Du, S., Zhang, T.: Small-size broadband coding metasurface for RCS reduction based on particle swarm optimization algorithm. Prog. Electromagn. Res. M **81**, 97–105 (2019)

Malhat, H.A., Badawy, M.M., Zainud-Deen, S.H., Awadalla, K.H.: Dual mode plasma reflectarray/transmitarray antennas. IEEE Trans. Plasma Sci. **43**(10), 3582–3589 (2015)

Paquay, M., Iriarte, J.C., Ederra, I., Gonzalo, R., de Maagt, P.: Thin AMC structure for radar cross-section reduction. IEEE Trans. Antennas Propag. **55**(12), 3630–3638 (2007)

Singh, H., Jha, R.M.: Active Radar Cross Section Reduction: Theory and Applications, 1st edn. Cambridge University Press, Cambridge (2015)

Singh, G., Marwaha, A.: A review of metamaterials and its applications. Int. J. Eng. Trends Technol. **19**(6), 305–310 (2015)

Song, T., Cong, L.L., Tong, C.M.: Ultra-wideband robust RCS reduction with triangle-type AMC structure. Radio Eng. **27**(2), 402–208 (2018)

Zainud-Deen, S.H., Malhat, H.A., Shabayk, N.: Radar cross section reduction using perforated dielectric material and plasma AMC structure. In: National Radio Science Conference, (NRSC 2018), Cairo, Egypt (2018).

Zainud-Deen, S.H., Badawy, M.M., Malhat, H.A.: Dielectric resonator antenna loaded with reconfigurable plasma metamaterial polarization converter. Plasmonics **14**(6), 1321–1328 (2019)

Zhang, J.J., Wang, J.H., Chen, M., Zhang, Z.: RCS reduction of patch array antenna by electromagnetic band-gap structure. IEEE Antennas Wirel. Propag. Lett. **11**, 1048–1051 (2012)